Environmental Science Nano

Proteomic, gene and metabolite characterization reveal uptake and toxicity mechanism of cadmium sulfide quantum dots in soybean plants

Journal:	*Environmental Science: Nano*
Manuscript ID	EN-ART-05-2019-000599.R1
Article Type:	Paper
Date Submitted by the Author:	20-Aug-2019
Complete List of Authors:	Majumdar, Sanghamitra; University of California Santa Barbara, Bren School of Environmental Science and Management Pagano, Luca; University of Parma, Dept. Chemistry, Life Sciences and Environmental Sustainability Wohlschlegel, James; UCLA, Department of Biological Chemistry, David School of Medicine Villani, Marco; Institute of Materials for Electronics and Magnetism National Research Council Zappettini, Andrea; Institute of Materials for Electronics and Magnetism National Research Council White, Jason; Connecticut Agricultural Experiment Station Keller, Arturo; University of California Santa Barbara

Environmental Significance Statement

The underlying mechanism of entry of nanoparticles into plants and their associated biological response is not well understood. This study addresses cellular and molecular level understanding of the processes in soybeans, a major agricultural crop, when exposed to bare as well as coated cadmium sulfide quantum dots using advanced bioanalytical and biostatistical tools. The global proteome, metabolites and gene expression in the quantum dot-exposed plants are also compared with those exposed to soluble cadmium compound and bulk-equivalent of cadmium sulfide to identify nanomaterial-specific response. The finding clearly suggest that the quantum dots activate defense response and transporter system in the soybean plants which is not entirely due to the dissolution of cadmium ions.

Proteomic, gene and metabolite characterization reveal uptake and toxicity mechanism of cadmium sulfide quantum dots in soybean plants

Sanghamitra Majumdar[1,2], Luca Pagano[3], James A. Wohlschlegel[4], Marco Villani[5], Andrea Zappettini[5], Jason C. White[6], Arturo A. Keller[1,2]*

[1]Bren School of Environmental Science and Management, University of California, Santa Barbara, CA 93106, United States

[2]University of California, Center for Environmental Implications of Nanotechnology, Santa Barbara, CA 93106, United States

[3]Department of Chemistry, Life Sciences and Environmental Sustainability, University of Parma, Parma 43124, Italy

[4]Department of Biological Chemistry, David School of Medicine, University of California, Los Angeles, CA 90095, United States

[5]Institute of Materials for Electronics and Magnetism (IMEM-CNR) Parma, Italy

[6]Department of Analytical Chemistry, The Connecticut Agricultural Experiment Station, New Haven, CT 06504, United States

***Corresponding author**

Dr. Arturo A. Keller

Bren School of Environmental Science & Management

University of California,

Santa Barbara, CA 93106

Office: (805) 893-7548

Mobile: (805) 453-1822

Email: keller@bren.ucsb.edu

Abstract

Nanomaterial-specific response of quantum dots and the underlying mechanisms of their interaction with plants is poorly understood. In this study, we investigated the mechanism of cadmium sulfide-quantum dot (CdS-QD) uptake and stress response in soybean (*Glycine max*) plants using sensitive bio-analytical techniques. We adopted shotgun-proteomics and targeted analysis of metabolites and gene expression in the tissues of soybean plants exposed to 200 mg/L CdS-QDs in vermiculite for 14 days. The molecular response in the soybeans as a function of surface coatings on CdS-QDs, specifically, trioctylphosphine oxide, polyvinylpyrrolidone, mercaptoacetic acid and glycine was also tested. The biological response of CdS-QDs was compared to Cd-ions and bulk-CdS to identify nanomaterial-specific response. The transmembrane proteins involved in uptake and genes including NRAMP6 and HMA8 were regulated differently in CdS-QD-treated plants compared to Cd-ion-treated plants. The ATP-dependent ion-transporters in the membranes presented feedback mechanisms in the soybean roots to restrict the uptake of CdS-QDs and simultaneously altered the mineral acquisition. CdS-QDs perturbed major metabolic pathways in soybean including glutathione metabolism, tricarboxylic acid cycle, glycolysis, fatty acid oxidation and biosynthesis of phenylpropanoid and amino acids. This study provides clear evidence that that the toxic responses and tolerance mechanisms in plants is specific to CdS-QDs exposure, and not entirely due to leaching of Cd ions.

INTRODUCTION

Over the past decade, a diverse range of engineered nanomaterials (ENMs) have been incorporated in electronics, agrochemicals, medicines, and consumer products without a comprehensive understanding of their use-release dynamics and long-term impact on the environment (1). Harnessing maximum benefits from nano-enabled products requires a thorough understanding of their interactions with the biological components in the environment, followed by careful considerations of the potential risks to human health. The dynamic interactions at the nano-bio interface are controlled by physicochemical and thermodynamic reactions between the nanocolloid surface and the biological milieu composed of proteins, metabolites, organelles, phospholipid membranes, and genetic material (2). In order to gain a resolved view of the mechanisms at the interface, advanced bio-analytical and "omic" techniques have been applied to identify sensitive endpoints of ENM exposure and tolerance in biological species (3). The development of mass spectrometry (MS) has significantly improved the throughput of detection and quantification of small and large molecules in biological matrices.

The global protein and metabolite profile of an organism with relative quantification strategies can provide a mechanistic perspective on the complex processes associated with phenotypic expressions in response to external stimuli. Proteomic characterization of ENM-treated plants can identify the proteins and associated interactions that are differentially regulated in response to ENM exposure, providing a link between altered gene expression and metabolic processes (4). In addition, analysis of plant metabolites provides snapshots of the biochemical processes modulated by ENMs exposure under specific environmental condition. An integrated approach efficiently provides a holistic overview of the signaling processes and biological pathways regulated by ENMs (5, 6). An untargeted approach in systems biology enables

screening for biomarkers of exposure which can be subsequently validated by targeted analysis of the biomolecules.

Quantum dots (QDs) are nanocrystals with exceptional optical properties that typically consist of a semiconductor core like cadmium sulfide (CdS), cadmium selenide (CdSe), or cadmium telluride (CdTe), often coated with an outer shell to prevent surface oxidation of the core, leaching of Cd^{2+}, and improving photoluminescence, quantum yield and colloidal stability (7). The surface of QDs can be easily modified with ligands depending on desired applications that range from biomedical imaging and drug delivery to light emitting diodes in displays, lighting, and photovoltaics (7, 8). Nevertheless, a significant fraction of the QDs released during use, disposal or recycling of electronic devices and medicinal applications accumulate in landfills and biosolids at ng/kg to μg/kg levels, which threatens the safety of agricultural crops unintendedly exposed to contaminated soil and water sources (9). According to previous studies in microbes and aquatic plant species, toxicity of Cd-based QDs is attributed to Cd^{2+} release; but, most studies have based this conclusion by comparing biological responses to QDs and soluble Cd-compounds with similar doses or equivalent total Cd content (10, 11). However, only a small fraction of Cd^{2+} from QDs is dissolved in contrast to soluble Cd-compounds at equimolar Cd concentrations (12). Hence, the Cd availability from QDs is generally overestimated and the specific mechanism of toxicity of QDs remains unclear. In a planktonic bacteria (*Pseudomonas aeriginosa*), CdSe QDs were found to be more toxic by generating more intracellular reactive oxygen species (ROS) than soluble Cd salts, at equivalent Cd concentrations of 20-125 mg/L (13). This study suggested that the toxic responses to QDs were distinct from soluble Cd salts, and thus were attributed to factors more than just the availability of Cd^{2+} ions.

There is limited knowledge on the mechanisms of subcellular transport and toxicity of Cd-based QDs in plants, and the findings from Cd^{2+} toxicity studies are not applicable due to unique material properties and dynamic biophysical interactions at nanoscale (14-17).Using gene expression analysis of Cd-tolerant mutant lines and genome-wide transcriptomics, *Arabidopsis thaliana* ecotypes exposed to CdS-QDs exhibited differential regulation of genes encoding antioxidant enzymes, anthocyanin production, trichoblast differentiation, root development pathways, photosynthesis, sulfur transport, metal chelation, and phenylpropanoid synthesis (18). However, the choice of QD surface coating plays a decisive role in the process of adherence, dissolution, biological uptake and interactions at the nano-bio interface (19-23). Soybean (*Glycine max*) is an important leguminous crop cultivated worldwide and is a major nutritional source of protein, oils, and carbohydrates (24). In a recent study, we exposed soybean plants to CdS-QDs without any coating or coated with different ligands including a water-soluble polymer (polyvinypyrrolidone, PVP), a hydrophobic ligand (trioctylphosphine oxide, TOPO), a thiol compound (mercaptoacetic acid, MAA) and an amino acid (glycine, GLY) in vermiculite media (12). Exposure to CdS-QDs coated with MAA or GLY resulted in Cd accumulation in soybean root cell walls, whereas CdS-QDs coated with TOPO were unstable due to the hydrophobicity of the ligand and released Cd^{2+} ions that accumulated in cell membranes. In contrast, PVP coating on the CdS-QDs enabled efficient transport of the particles or Cd^{2+} to root organelles and aerial tissues, leading to reduced leaf biomass. The study showed that lignification and amino acid (AA) regulation play an important role in stress tolerance in plants upon exposure to CdS-QDs, which necessitates further understanding at the molecular level.

The aim of the current study was to elucidate the cellular and molecular mechanisms involved in the uptake and stress tolerance of CdS-QDs in soybeans as a factor of surface

coating, and identify nano-specific response by comparing with bulk-CdS or soluble Cd-compound exposures. A label-free proteomic analysis of roots and targeted analysis of metabolites (AAs, organic acids, and antioxidants) in roots and shoots were performed following a 14-day exposure. Transcriptional analysis of Cd-responsive genes in roots and shoots was performed using Real-Time Quantitative Reverse Transcription PCR (qPCR). An integration of the proteomic profile with metabolite accumulation and gene expression in soybean plants exposed to CdS-QDs was conducted to corroborate the hypothesis generated by untargeted proteomics on the involvement of specific biological pathways in the roots.

MATERIALS AND METHODS

Synthesis and stability of cadmium sulfide-quantum dots

Uncoated CdS-QDs (QD-BARE) were synthesized following Villani et al. (25) and then modified at the surface using TOPO, PVP, MAA, or GLY resulting in QD-TOPO, QD-PVP, QD-MAA and QD-GLY, respectively (12). All the synthesized CdS-QDs were smaller than 8 nm in diameter and attenuated total reflectance-fourier transform infrared spectroscopy (ATR-FTIR) confirmed the presence of the surface coatings on the particles, as discussed in our previous complementary work focused on the stability and characterization of these particles (12).

To study the stability of particle in suspension in pristine or natural condition, 100 μg/ml uncoated or coated CdS-QDs were prepared in Milli-Q-water (MQW) or fresh root exudates. Soybean root exudates was collected by immersing the roots of 11day old soybean seedlings in MQW for 6 h (pH= 5.4 ± 0.2). The CdS-QDs were suspended in MQW or extracted root exudates by probe sonication at 40% amplitude for 2 min (Fisher Scientific Model 505 sonic dismembrator, Waltham, MA, USA). The average size (hydrodynamic diameter) and zeta (ζ)

potential of the suspended CdS-QDs were measured immediately in triplicates using a Zetasizer Nano ZS (Malvern Instruments, Worcestershire, United Kingdom). Percent dissolution of the CdS-QDs was calculated with respect to the total Cd content measured in the aliquots of the suspensions after 24 h of preparation. To determine the dissolved Cd^{2+} ion fraction, respective aliquots were passed through Amicon 3KDa centrifugal filters for 2 h at 3000 rpm in an Eppendorf 5810 centrifuge and acidified with 2 ml concentrated HNO_3 and 0.5 ml H_2O_2; the final solutions were diluted to 5% HNO_3. The acidified solutions were analyzed for Cd content by inductively coupled plasma-optical emission spectrometry (ICP-OES, iCAP 6500, Thermo Fisher Scientific, Waltham, MA).

Plant exposure to cadmium sulfide quantum dots

Soybean (*Glycine max* var. Tohya) seeds purchased from Johnny's Selected Seeds (Albion, ME, USA), were washed with 1% sodium hypochlorite solution, rinsed thoroughly and soaked in MQW for 24 h. Seeds were germinated in vermiculite and 11-day old seedlings were each planted in 40 ml (~6 g) of untreated (CTRL) or treated vermiculite in 50 ml tubes. The treatments were 200 μg CdS-QDs per ml of vermiculite (QD-BARE, QD-TOPO, QD-PVP, QD-MAA, and QD-GLY), 100 μg/ml bulk-CdS (BULK), and 10 μg/ml $CdCl_2$ (ION). Each treatment group included three replicates with two plants per replicate. The treatments were prepared in 12 ml MQW (water holding capacity of 6 g vermiculite) by probe sonication and were homogeneously mixed with vermiculite. The findings from our previous study suggested that most prominent impacts on growth, root architecture, lignification and oxidative stress were noted in soybean plants exposed to CdS-QDs at 200 μg/ml (12). Hence, this dose was selected for further mechanistic studies. The BULK exposure at 200 μg/ml was toxic for the plants resulting in unhealthy and withering plants, thus 100 μg/ml was used for comparison. The ION

treatment was established at 10 μg/ml to account for ~5% dissolved Cd fraction from the CdS-QDs, as determined from dissolution experiments. The plants from all treatment groups were grown simultaneously under 16 h photoperiod (light intensity 120 μM m^{-2} s^{-1} photosynthetic photon flux) at 24 °C and 30% relative humidity. The plants were irrigated with MQW as needed. After 14 days of exposure, the plants were harvested, washed with MQW, and divided into roots and shoots. The tissues from two plants in each replicate were combined, immediately finely ground in liquid nitrogen and stored at -80 °C for further analysis of proteins, metabolites, gene expression.

Proteomic analysis

LC-MS/MS analysis of peptides. To investigate the interaction of transport proteinss with CdS-QDs and alteration of biological pathways in the tissues directly in contact with the particle, the proteins in soybean roots of each treatment group were extracted following Majumdar et al. (26). Trypsin-digested protein samples were analyzed by tandem mass spectrometry using a Thermo Easy-nLC system coupled to a Thermo Q-Exactive MS (27). The detailed procedure for sample preparation and liquid chromatography- tandem mass spectrometry (LC-MS/MS) analysis is provided in the Supporting Information Method S1. The MS proteomics data have been deposited in the ProteomeXchange Consortium via the PRIDE partner repository with the dataset identifier PXD013246 (28).

Protein identification and quantification. The relative label-free quantification (LFQ) of the acquired MS data for soybean root samples was carried out using the MaxQuant software (*v*.1.6.3.3) based on peak areas of the peptides derived from their intensity in the full mass scan as they were eluted into the mass spectrometer. Spectra were searched against the *G. max* UniProtKB database (89,466 entries; October 2018) using MaxQuant-integrated Andromeda

search engine for peptide identification (29). A minimum peptide length of 7 AAs and trypsin specificity was required for protein identification and maximum two missed cleavages were permitted. The false discovery rate (FDR) for peptide spectrum match and protein was set to 0.01. Oxidation of methionine (*Met*) residues and N-terminal acetylation were allowed as variable modifications. Carbamidomethylation of cysteine (*Cys*) residues was selected as a fixed modification. The precursor and fragment mass tolerance were set at 4.5 and 20 ppm, respectively. Proteins with at least two matched peptides and one unique peptide were considered valid for further analysis. A second round of database searching using co-fragmented peptides was included to increase the number of protein identifications. The isotope pattern of each peptide was matched across all runs on the basis of mass and retention time. Protein abundance in the roots was calculated based on normalized spectral intensities (LFQ intensity).

Proteomics data processing. The proteins identified and quantified in the soybean roots were processed for statistical analysis using Perseus software (*v*.1.6.2.3) (30). The LFQ intensities were filtered for *reverse*, *only identified by site* and *contaminant* peptides, and were log2(x) transformed. Proteins that were present in all three replicates in at least one group of treatment were considered valid and were used for further downstream analysis. The filtered values were subjected to analysis of variance (ANOVA) controlled by a Benjamini-Hochberg FDR ≤ 0.05 to identify the significant proteins. Principal component analysis (PCA) was performed on the total number of identified proteins and the ANOVA-significant proteins. The log2(x) transformed intensity values of the ANOVA-significant proteins were Z-scored and clustered into groups by hierarchical clustering analysis based on Pearson's correlation. Functional annotation and Gene Ontology (GO) of the identified proteins was performed using the UniprotKB and KEGG tools (31, 32).

Targeted analysis of metabolites

The frozen ground soybean tissues from each treatment group were extracted in 80% methanol containing 2% formic acid and used for detection and quantification of organic acids, AAs, and antioxidants using Agilent 1260 UHPLC binary pump coupled with Agilent 6470 triple quadrupole mass spectrometer as described in Method S2. The list of metabolites and the information on retention time, parent and product ions and linearity of the calibration curves are provided in Table S1.

Data acquisition and processing was performed using Agilent MassHunter software (*v.B.06.00*). Statistical analysis was performed using Metaboanalyst 4.0 (33). For multivariate analysis, log2(x) transformation and pareto-scaling were performed on the metabolite concentration values. An unsupervised PCA and a supervised partial least-squares-discriminant analysis (PLS-DA) were applied to the normalized data. One-way ANOVA followed by Fisher's LSD test (FDR ≤ 0.05) was performed to identify metabolites of interest.

Real Time qPCR analysis

Total RNA was extracted from soybean root and shoot tissues and reverse transcription was performed using the Qiagen QuantiTect Reverse Transcription kit (Qiagen, Velno, Netherlands). Fourteen sequences of soybean ortholog genes were chosen due to their reported involvement in transport of Cd in soybeans and response to CdS-QDs in *A. thaliana* (18). A detailed description of the qPCR analysis is provided in Method S3. The information on the genes and primer sequences are reported in Table S2. Univariate statistical analysis was performed for the qPCR results using two-tail Student's t-test. The data presented is the log-normalized relative expression fold change of genes in the exposed soybean tissues with respect to CTRL.

Bioinformatics and pathway analysis

The differentially accumulated proteins (DAPs) in the roots exposed to CdS-QDs were used for protein-protein interaction (PPI) analysis using STRING database (https://string-db.org; *v.*11.0) with a high-confidence interaction score (≥ 0.7) and associated pathway enrichment was performed with respect to the *G. max* database (34). Network was constructed by integrating differentially regulated proteins, genes and metabolites using Cytoscape (*v*.3.7.1) (35).

RESULTS AND DISCUSSION

Stability of bare and coated CdS-QDs in suspension

In MQW, the hydrodynamic diameter of QD-BARE (550 ± 16 nm) and QD-MAA (306 ± 2 nm) agglomerates was significantly smaller than QD-TOPO (1133 ± 62 nm), QD-PVP (950 ± 20 nm) and QD-GLY (884 ± 24 nm) (Table S3) . The large size of QD-TOPO in aqueous media is attributed to the hydrophobicity of the long alkyl chains in TOPO molecules (12). Interestingly, all the CdS-QDs were stabilized in root exudates, with size ranging from 314 to 347 nm, except QD-TOPO, which formed agglomerates measuring 1233 ± 13 nm. The improvement in the stability of QD-BARE, QD-PVP, QD-MAA, and QD-GLY in the presence of root exudates was also confirmed by the higher negative ζ-potential values (-24 to -28 mV) compared to -5 to -23 mV when suspended in MQW. In contrary, the ζ-potential of QD-TOPO suspended in MQW and root exudate was -13.8 and -17.5 mV, respectively (Table S3). These observations suggest formation of biocorona around the CdS-QD aggregates in the presence of root exudates, resulting in lesser affinity between particles; hence, less aggregation and enhanced colloidal stability under plant's influence. Previous studies have also reported that natural amphiphilic compounds present in algal exudates form biocorona around graphene and graphene oxide sheets, depending on their binding affinity to the particles (36). Interestingly, the

dissolution percentage of Cd^{2+} ions from QD-TOPO was significantly lowered when suspended in root exudates (1.5%) compared to MQW (9.8%) (Table S3). The Cd^{2+} dissolution from QD-BARE, QD-PVP, and QD-GLY also decreased to 3-5% when suspended in root exudates compared to 9-11% in MQW. On the other hand, QD-MAA released 5% Cd^{2+} in either MQW or root exudates, demonstrating stability. Based on the dissolution results, the dose of the soluble Cd compound (10 μg/ml) to investigate the comparative response of soybean plants was selected at 5% of the tested concentration of CdS-QDs (200 μg/ml).

Global proteomic profiling in soybean roots

Label-free proteomic analysis of the soybean roots identified a total of 23,994 peptides corresponding to 3,511 protein groups across all treatments. A PCA score plot considering all identified proteins showed a clear separation between CTRL and Cd treatments along component 1 (Figure S1). A total of 1974 proteins were validated by their presence in all the replicates of at least one treatment and were considered as *high-confidence proteins* (Table S4). Multi-scatter analysis was performed to examine the reproducibility of the quantification among the triplicates in each treatment groups. The average Pearson's correlation coefficient of the replicates within each treatment was ≥ 0.96, suggesting a high degree of correlation (Figure S2).

An average of 1846, 1897, 1915, 1895, 1896, 1876, 1809 and 1809 proteins were detected in the roots exposed to CTRL, ION, BULK, QD-BARE, QD-TOPO, QD-PVP, QD-MAA, and QD-GLY, respectively. A total of 1690 proteins were common between the different CdS-QD treatments (Figure 1a) and 1594 proteins were common between all the treatments (Figure 1b). Among proteins identified in the roots, 22 were exclusively expressed in one or more CdS-QD treatments (Table S5). Analysis of GO terms suggest that these unique proteins in CdS-QD-treated roots are localized in the cell wall, extracellular region, or integral components

of membranes/membrane-bound organelles, involved in transmembrane transport of metal ion or protons, chitin binding, carbohydrate metabolism, and response to oxidative stress (Table S5). A peroxisome-localized uricase-2 isozyme-1 was found unique to QD-BARE, QD-TOPO, QD-MAA and QD-GLY-treated roots. In legumes, uricases play an important role in nitrogen fixation by catalyzing the ultimate step of purine oxidation to ureides (37). Pectinesterase, an enzyme involved in cell wall modification was uniquely found in QD-PVP and QD-GLY-treated roots. A total of 65 proteins were found in common between ION, BULK and CdS-QDs, of which 54 proteins were involved in catalytic activities (Table S6). Pathway enrichment of these proteins identified 18 metabolic pathways involved in glutathione (GSH) metabolism, carbon metabolism, AA metabolism, and biosynthesis of secondary metabolites including isoflavonoids, phenylpropanoids, isoquinoline alkaloids, and monoterpenoids.

One-way ANOVA of the high-confidence proteins identified 538, 285 and 119 differentially accumulated proteins (DAPs) between treatments at FDR $\leq$ 0.05, 0.01, and 0.001, respectively (Table S4). The PCA score plot for the 538 DAPs clearly shows that proteins from CdS-QD-treated roots were well separated from CTRL, ION and BULK, explained by a variance of 67% along component 1 (Figure 2a). QD-PVP- regulated proteins were separated from the other CdS-QDs along component 2. In comparison to CTRL, the treatments resulted in 58 (ION), 201 (BULK), 321 (QD-BARE), 245 (QD-TOPO), 328 (QD-PVP), 351 (QD-MAA), and 300 (QD-GLY) DAPs in the roots (Fig. 2b-d). Hierarchical clustering analysis grouped the DAPs into three clusters based on abundance (Figure 3a,b). Cluster-1 only had 9 proteins that showed higher abundance in QD-MAA and QD-GLY treatments compared to QD-BARE and BULK. Cluster-2 proteins showed decreased abundance in the CdS-QDs treatments compared to CTRL and ION, while Cluster-3 proteins showed higher abundances in CdS-QDs and BULK treatments

than CTRL and ION (Figure 3b). The clustering analysis of the treatment groups clearly separated ION from CdS-QD treatments (Figure 3a) suggesting nanoscale-specific response at the proteome level in the CdS-QD- exposed soybean plants.

Cadmium sulfide-quantum dots induce unique proteomic response in soybean roots

Compared to CTRL, 276 and 204 proteins in the CdS-QD exposed roots showed increased and decreased abundances, respectively (Figure 2), corresponding to 35 and 20 pathways determined by functional enrichment using STRING database (Table 1). A total of 99 proteins were over-accumulated in all the CdS-QD-treated roots as compared to CTRL, irrespective of surface coating (Figure 2d), out of which 25 proteins were unique to CdS-QD treatments and were not differentially accumulated in ION or BULK-treated roots, thus demonstrating nanoscale-specific responses (Table S7). Mapping these CdS-QD-specific over-accumulated proteins in KEGG pathway suggested upregulation of intermediary steps in glycolysis (3-phospho-D-glycerate→2-phospho-D-glycerate; pyruvate→acetyl Co-A) and TCA cycle (isocitrate→2-oxoglutarate), urate oxidation and ATP synthesis-coupled-proton transport. Proteins involved in β-oxidation of fatty acids and biosynthesis of jasmonic acid and sphingosine were also over-accumulated in the CdS-QD-treated roots, suggesting upregulation of stress signaling pathways (38). In addition, enhanced stress was also demonstrated by upregulation of phenylpropanoid pathway, specifically lignin biosynthesis. A total of 52 over-accumulated proteins were common between BULK and CdS-QDs-treated roots, but not in ION exposures (Table S7). Pathway mapping of these 52 proteins demonstrated upregulation of biosynthesis of intermediates in pentose phosphate pathway, glucoronate pathway, Calvin and TCA cycle, glycolysis/gluconeogenesis, biosynthesis of serine (*Ser*), tyrosine (*Tyr*) and branched chain AAs, catecholamine biosynthesis, gamma-aminobutyrate (GABA) shunt, phenylpropanoid pathway,

GSH metabolism, and isoflavonoid synthesis. In addition to these, compared to CTRL, 22 proteins were over-accumulated in the roots of CdS-QDs, BULK and ION treatments, which reflect the response to Cd^{2+} ions released from the CdS-QDS. These were specifically involved in *Cys* biosynthesis, TCA cycle (Citrate←→Isocitrate; 2-oxoglutarate→Succinyl Co-A), carbon fixation, glyoxylate/dicarboxylate metabolism, jasmonic acid biosynthesis, and terpenoid biosynthesis (*β*-carotene→abscisic acid). Out of the 204 under-accumulated proteins in CdS-QD exposed roots, 44 were common to all the CdS-QD-treated roots (Figure 2d). Among these, 19 proteins were unique to CdS-QD exposures (Table S7), which were involved in defense response, ion binding, channel activity, membrane organization and biosynthesis of 1,3 β-D-glucan. Calcium-transporting ATPase activity was also downregulated in all CdS-QD-treated roots. In addition, 22 proteins were under-accumulated only in BULK and CdS-QD-exposed roots, which were involved in defense response via peroxidases and cytochrome P-450, jasmonic acid biosynthesis, sucrose and starch catabolism, and biosynthesis of phenylpropanoid pathway intermediates (coumarinate, p-coumaroyl shikimic acid, p-coumaroyl quinic acid and caffeoyl-CoA).

The surface coating of the CdS-QDs also influenced the proteomic response in soybean roots (Table S7). Pectinesterases involved in cell wall modification, malonyl-CoA in fatty acid metabolism, and a class of γ-GST were over-accumulated only in plants exposed to QD-GLY, QD-PVP and QD-MAA; whereas glutamate dehydrogenase was over-accumulated in plants exposed to QD-PVP and QD-TOPO. Exposure to QD-MAA and QD-GLY resulted in the under-accumulation of Cu-ion binding amine oxidase and γ-glutamyl hydrolase, which is involved in regeneration of *Glu*, and the over-accumulation of pyruvate kinase and glyceraldehyde-3-phosphate dehydrogenase involved in glycolysis. Plants treated with QD-BARE uniquely over-

accumulated 3Fe-4S cluster binding proteins involved in *Glu* biosynthesis, and proteins involved in histidine (*His*) metabolism and phosphoric diester hydrolase activity in lipid metabolism; whereas under-accumulated proteins responsible for ATP-binding and cell wall-associated beta-glucosidase activity that hydrolyzes isoflavonoid glycosides to release monolignols (39). Compared to other CdS-QDs, QD-TOPO treatment uniquely over-accumulated mechanosensitive ion-channel protein in the roots, similar to BULK. QD-PVP-treatment exclusively resulted in over-accumulation of 13 proteins in the roots, including two major stress enzymes, catalase and glutathione reductase, a Fe-S protein (ferredoxin) involved in electron transfer activity, Mn-ion binding aminopeptidases, and Co- or Zn-ion binding proteins involved in allantoinase activity as a part of nitrogen fixation. In addition, QD-PVP-exposed roots exclusively under-accumulated 12 proteins involved in binding to nucleic acid, nucleotides/nucleosides, carbohydrates or anions. In the QD-MAA-exposed roots, several oxidoreductase enzymes, including GST and carboxypeptidase (proteases) were over-accumulated, and GSH synthetase, S-(hydroxymethyl) glutathione dehydrogenase, and superoxide dismutase were under-accumulated. QD-GLY treatment uniquely resulted in differential accumulation of ATP and GTP-binding proteins, and decreased abundance of α-galactosidases.

Altered gene and metabolite response in soybean roots

Pathogenesis related gene (PR1) present in plant cell wall and extracellular region, is conserved across the plant kingdom and is involved in defense response through systemic acquired resistance pathways (40). PR1 gene in the roots was upregulated by 4-6 fold in all the treatments, compared to CTRL (Figure 4a, Table S8). In plants, GSH plays a major role in the detoxification of metals like Cd or As with high affinity for thiol compounds (41). The

biosynthesis and degradation of GSH occurs through the γ-glutamyl cycle and is initiated by γ-glutamyl transpeptidase (GGT), a membrane bound non-cytosolic protein which cleaves γ-glutamyl bond to generate Cys-Gly dipeptides and γ-glutamyl AAs (42). γ-Glutamylcyclotransferases (GGCTs) in the cytosol then converts γ-glutamyl AAs to 5-oxoproline, which then recycles *Glu* for GSH synthesis. The GGCT2;1 gene encodes the γ-glutamyl cyclotransferase ChaC-like protein and is involved in GSH homeostasis. In roots, GGCT2;1 was significantly downregulated in all the CdS-QD and BULK treatments which correlates with the accumulation of a significant amount of Cd in the soluble fraction (cytoplasm and vacuoles) (33 ± 4 to 49 ± 10 μg/g in CdS-QD and 14 ± 0.8 μg/g in BULK-treated roots) (Figure 4a, Table S9); however, it was not significantly affected in the ION treatments due to low level of Cd (2 ± 0.6 μg/g) in the soluble fraction (12).

A heavy metal-associated isoprenylated plant protein (HIPP22), expressed in lateral root tips, is known to be involved in Cd^{2+} transport and homeostasis (43). In the soybean roots, HIPP22 was downregulated across all Cd treatments; the downregulation was 2-fold in the ION, QD-MAA, and QD-GLY treatments, and 3 to 3.5-fold in the BULK, QD-BARE, QD-TOPO and QD-PVP treatments. Heavy metal transporters, NRAMP6 and HMA8, and the tonoplast intrinsic protein TIP2;1 were downregulated only in the CdS-QD-exposed roots. NRAMP6 was downregulated in the roots from QD-PVP, QD-MAA and QD-GLY by ~6-fold; however, its expression was enhanced in the ION-exposed roots. QD-BARE, QD-TOPO and QD-PVP downregulated the HMA8 expression by 4, 10 and 3-fold, respectively. QD-BARE and QD-PVP exposures also resulted in the downregulation of the aquaporin gene, TIP2;1, which is responsible for water transport from vacuoles to the cytoplasm (Figure 4a).

Targeted analysis of three groups of plant metabolites including antioxidants, organic acids and AAs using LC-MS/MS identified 23 compounds in the soybean roots (Table S1). An unsupervised PCA score plot of the identified metabolites shows that the CdS-QD treatments were separated from CTRL along component 2, explaining a variance of 20.9% (Figure 5a). The analyzed metabolites in CdS-QDs were well separated from the ION along component 1. Further, supervised PLS-DA plot clearly suggests that the CdS-QDs had a nanoscale-specific response on the accumulation of metabolites in the soybean roots, compared to ION and BULK (Figure 5b). Ten metabolites with a VIP score ≥ 1 were identified as important variables responsible for the separation of the treatment groups in the PLS-DA model (Figure 5c). Compared to CTRL, *Glu* content in the CdS-QD-treated roots was significantly over-accumulated by fold of 9 (QD-BARE), 11 (QD-TOPO), 5 (QD-PVP), 21 (QD-MAA), and 12 (QD-GLY), whereas by 2 and 4-fold in ION and BULK-treated roots, respectively (Table S10). This also corroborates the finding in gene expression studies where GGCT2;1 is downregulated, resulting in accumulation of γ-glutamyl-AAs. In addition, tryptophan (*Trp*) was also over-accumulated in all the CdS-QD-exposed roots by 2- to 3-fold, whereas ION exposure led to a 2-fold decrease compared to CTRL (Table S10). The aromatic AAs, *Trp*, phenylalanine (*Phe*) and tyrosine (*Tyr*) are initiated from metabolites of glycolysis and pentose phosphate pathway via the shikimate pathway and are involved in the biosynthesis of various metabolites including phenylpropanoids. Tryptophan is a precursor of indole-containing secondary metabolites, like plant hormone auxin (indole-3-acetic acid), glucosinolates and indole-alkaloids (44).

ION exposure resulted in significantly decreased accumulation of most root metabolites (Figure 5d, Table S10). Proline (*Pro*) was reduced in the roots from the BULK and ION treatment; however, did not affect the CdS-QD exposed roots. Compared to CTRL, the

accumulation of lysine (*Lys*), arginine (*Arg*), *His* and aspartic acid (*Asp*) decreased exclusively in the ION-exposed roots. Aspartic acid is involved in the biosynthesis of alanine (*Ala*) and *Arg*, and both of them contribute to *Lys* biosynthesis. The under-accumulation of AAs and organic acids in the ION-exposed roots in addition to the enhanced regulation of NRAMP6 which is involved in intracellular Cd^{2+} mobility, highlights the sensitivity to Cd^{2+} even at significantly low Cd accumulation in the roots (Table S9). *Ser*, *Phe*, and *Ala* were under-accumulated in the BULK and ION-exposed roots, but also showed significant decrease in levels in QD-PVP-exposed roots. Threonine (*Thr*) and glycine (*Gly*) were under-accumulated in the BULK, ION, QD-PVP, QD-TOPO and QD-GLY-exposed roots. The roots from all the Cd treatments resulted in the decreased accumulation of *Met*, valine (*Val*), and leucine (*Leu*). In addition, benzoic acid and caffeic acid contents decreased in the CdS-QDs and ION-exposed roots. *Cys* content in the roots significantly decreased by $\geq$ 1.5-fold only in the CdS-QD exposures (Table S10).

Altered gene and metabolite response in soybean shoots

In the soybean shoots, PR1 gene was upregulated in all the Cd treatments by 1.1 to 2.6-fold (Figure 4b), suggesting activation of systemic acquired resistance in response to Cd accumulation in the apoplast (Table S9). Similar to the roots, GGCT2;1 was also downregulated (1.4 to 2.9-fold) in the shoots of CdS-QD and BULK-treated plants (Figure 4b). Metallothioneins (MT) are *Cys*-rich low-molecular mass proteins that are also involved in plant stress tolerance to metal ions like Zn^{2+}, Cd^{2+} and Cu^{+} (45). The expression of the MT2 gene encoding MT type-2B protein was upregulated in the leaves of the QD-BARE, QD-PVP and QD-MAA treatments. The expression of the sulfate transporter gene, SULTR4;2 was downregulated by 2-fold in the BULK-exposed shoots similar to QD-TOPO treatment, but was upregulated by 3- to 4-fold in the QD-PVP, QD-MAA and QD-GLY-exposed shoots. Exposure to CdS-QDs resulted in

downregulation of the aquaporin gene (TIP2;1) unlike in ION treatments, with significant downregulation in QD-BARE, QD-TOPO and QD-MAA treatments suggesting gating of the aquaporin channels (Fig. 4b). HIPP22 gene involved in metal binding and transmembrane transport of ions was significantly downregulated by 2- to 3-fold in the shoots of soybean plants exposed to BULK and the coated CdS-QDs. QD-PVP exposure resulted in maximum downregulation of GGCT2;1 and upregulation of PR1 and SULTR4;2 among all the treatments, in addition to a significant increase in MT2 expression (Fig. 4b). Among the CdS-QD treatments, QD-MAA exposure uniquely upregulated PRR5, which encodes a pseudo-response regulator-5 protein involved in plant circadian rhythms.

A total of 26 metabolites were identified in the soybean leaves (Table S1). Although the separation of the treatment groups is not apparent in the PCA plot (Figure 6a), the three-dimensional view of the PLS-DA score plot shows that the CdS-QD groups (except QD-GLY) were distinct from CTRL and ION (Figure 6b). Eleven features with VIP score ≥ 1 were responsible for the separation between groups (Figure 6c). Sixteen metabolites were identified as significantly different in CdS-QD-exposed leaves compared to CTRL, but BULK and ION exposure did not affect the leaf metabolites significantly (Figure 6d). In the CdS-QD-treated shoots, eight AAs including *Glu*, *Gly*, *Lys*, *Pro*, *Ser*, *Thr*, *Tyr*, and *Val* showed more than 2-fold modulation in their abundance with respect to the CTRL (Table S11). QD-PVP exposure significantly enhanced the accumulation of *Arg* in the leaves, unlike other CdS-QDs. Among all CdS-QDs, QD-PVP exposure also resulted in maximum over-accumulation of *Asn* (1.3-fold), *Gly* (2.1-fold), *His* (1.7-fold), and *Lys* (3.4-fold). The abundance of *Glu* in the shoots was decreased by 2.2-fold only in the QD-PVP-exposed plants, which could be attributed to high Cd content in the soybean shoots (Table S9), triggering stress response signaling pathways. In all the

CdS-QD-exposed leaves, *Ser*, *Thr*, and *Gly* were over-accumulated by 1.4- to 2.6-fold. Although some leaf metabolites in QD-GLY treatments behaved similar to the other CdS-QDs, the abundance and regulation of *Arg*, *Glu*, *Leu*, and *Lys* were similar to ION treatments. The accumulation of malic acid in the leaves were enhanced by 1.6-fold only in the QD-MAA and QD-GLY treatments.

Integration of soybean proteome, metabolites and genes involved in CdS-QD response

The integration of the 315 "nodes", representing differentially-regulated biomolecules including proteins, metabolites and genes in the soybean roots exposed to CdS-QDs revealed that 149 nodes were connected with an average of four neighboring nodes, resulting in enrichment of 45 biological pathways (Figure 7). The major pathways that were affected by CdS-QDs were associated with biosynthesis of amino acids and phenylpropanoids, GSH metabolism and carbon metabolism including TCA cycle and glycolysis. The two downregulated genes, TIP2;1 and GGCT2;1, in the roots exposed to CdS-QDs were well connected with 19 and 3 neighbors respectively, which also showed decreased abundance and were involved in AA biosynthesis, ribosome biogenesis, *Cys* and *Met* metabolism, glycolysis, isoquinoline alkaloid biosynthesis, and GSH metabolism, respectively (Table S12). Higher number of neighbors of a node represent better connectivity to other biomolecules, and hence more influential in regulating biological response. Among the metabolites, *Glu*, *Phe*, *Cys*, *Gly*, *Ala*, *Asp* were the top candidates with ≥ 26 neighboring nodes. A CdS-QD-specific downregulated protein, EF1B-γ class glutathione-S-transferase interacted with 25 neighbors including the TIP2;1 gene. Several proteins involved in protein catabolism, ribosomal proteins and a citrate synthase also connected with ≥ 15 neighbors. Thus, the integration of the proteome with targeted metabolites and genes identified the candidates that control the responses in soybean plants exposed to CdS-QDs.

CdS-QDs employ unique transporter systems in soybean roots

In previous studies, confocal imaging techniques have provided evidence of transport of Cd-based QDs in plants (19, 22). However, these techniques do not provide the depth to unravel the molecular mechanisms that regulate their cellular uptake. In plants, Cd^{2+} enter through the epidermal layer in root tips and root hairs via transition metal ion transporters or channel proteins (46). Transporter proteins like ATP-binding cassette transporters (ABC), heavy metal-ATPases (HMA), natural resistance-associated macrophage proteins (NRAMP) families have been reported to participate in transport and homeostasis of a broad range of metal ions (47, 48). In our study, proteomic analysis of the roots revealed that a Cu-binding transmembrane metal transporter (A0A0R0LL96) and a phosphate transporter (Q8W198) were likely involved in Cd^{2+} transport in the roots exposed to the Cd treatments including ION, BULK, or CdS-QDs. In these roots, gene expression studies show a simultaneous downregulation of HIPP22 genes that are involved in the regulation of Cd-binding protein, which suggests a feedback mechanism in plants to restrict Cd uptake (49). Several membrane proteins related to P-P-bond-hydrolysis-driven protein transmembrane transport (I1MDC4) and metal-ion binding were over-accumulated in the roots exposed to BULK and CdS-QDs; whereas, ATPase-coupled Ca^{2+}-transmembrane transporter protein (K7LC34) was under-accumulated which may be responsible for limiting Cu transport to the leaves (Table S13). P-type ATPases are a class of integral membrane proteins which utilizes the energy from ATP hydrolysis to transport nutrients or metal ions across the plasma membrane for maintaining cellular homeostasis (50).

In our preceding study focusing on Cd and nutrient accumulation in soybean tissues, the CdS-QD exposures resulted in reduced Mg, Na, and Fe contents in the roots and Cu content in the leaves (Table S13) (12). Proteomics and gene expression analysis of the CdS-QD exposed

roots in the current study reveal the underlying processes involved in the alteration in the nutrient levels. In the CdS-QD-treated roots, two channel proteins (A0A0R0HUK1, A0A0R0L1G2) and a Mg-dependent ATPase-coupled Ca^{2+}-transporter (I1JGA0) were downregulated; simultaneously, two transporter genes, NRAMP6 and HMA8 were also downregulated. This suggests that the high Cd accumulation in the membrane fractions of the soybean roots exposed to CdS-QDs assigns ATP-dependent ion-channel proteins to restrict Cd transport to cytosol, which also affects mineral acquisition and distribution (51). Among the CdS-QD exposures, QD-BARE and QD-TOPO sequestered highest concentration of Cd in the membrane fractions (789 and 685 μg/g, respectively) (Table S9) that may have triggered maximum downregulation of these membrane transporters in order to protect the influx of Cd into the chloroplast. Homologues of NRAMP have also been previously implicated in transport and homeostasis of divalent metal ions (52). In *A. thaliana*, AtNRAMP6 was reported to be involved in intracellular Cd transport resulting in increased Cd sensitivity (53). Unlike CdS-QD treatments, the soybean roots exposed to ION treatments significantly upregulated the expression of the NRAMP6, which explains the high Cd content in shoots (12). Although the concentration of Cd in shoots of QD-PVP-exposed plants was significantly higher than the ION treated plant (Table S9), decreased NRAMP6 expression in the QD-PVP-treated roots suggests that it does not play a major role in the mobilization of the QD-PVP or constituent Cd^{2+} within the cellular compartments. Two transmembrane proteins (I1NF01, C6TCT4) were uniquely expressed in QD-BARE, QD-TOPO, QD-MAA and QD-GLY. Unlike other CdS-QDs, QD-TOPO treatment expressed a membrane-localized mechanosensitive ion-channel protein (K7LLZ5) in the roots similar to BULK. QD-MAA downregulated V-type proton ATPase subunit-a (I1LJ94) which is an essential component of the vacuolar proton pump that catalyzes the translocation of protons

across the membranes. Thus, the surface properties of the CdS-QDs influenced the transmembrane transport mechanisms in the soybean roots.

Aquaporins participate in water and ion transport, and maintain cellular homeostasis in response to abiotic stress (54). The downregulation of the aquaporin gene, TIP2;1, in the CdS-QD-exposed roots suggests interruption of solute transport through aquaporins. In maize seedlings, 72h exposure to lanthanide oxide nanoparticles also downregulated the expression of isoforms of aquaporin genes (55). The downregulation of HIPP22 and TIP2;1 in the aerial tissues of CdS-QD-exposed plants suggests defensive strategies to restrict Cd intracellular mobility.

CdS-QDs modulate energy and carbohydrate metabolism in soybean plants

A relatively short-term CdS-QDs exposure (14-days) to soybean roots induced cascades of feedback mechanisms that upregulated major metabolic pathways including glycolysis, TCA cycle, fatty acid β-oxidation, biosynthesis of amino acids, and biosynthesis of secondary metabolites. Glycolysis converts carbohydrates in the form of sucrose, fructose and UDP-glucose into pyruvate, which is further used as a substrate for the TCA cycle (56). The upregulation of the cytosolic proteins involved in the conversion of 3-phosphoglycerate to 2-phosphoglycerate and the oxidation of pyruvate to acetyl-Co-A was unique in CdS-QD-exposed roots. However, UTP:glucose-1-phosphate uridylyltransferase involved in regeneration of UDP-glucose from glucose-1-phosphate, as a part of glycogen metabolism, was downregulated in the CdS-QD-exposed roots similar to ION and BULK treatments, which suggests favorable utilization of glucose-1-phosphate in the glycolysis than glycogen metabolism. In the TCA cycle, all the Cd treatments upregulated the conversion of citrate to isocitrate in the roots; in addition, CdS-QDs uniquely stimulated the formation of succinyl co-A from 2-oxoglutarate. However, starch, sucrose and galactose metabolism were impaired in the CdS-QD-exposed roots similar to the

BULK and ION treatments. Xie et al. also reported that sugar utilization is hindered in bermudagrass (*Cynodon dactylon* Pers.) under Cd stress (57). Previous studies have reported that Cd exposure perturbs the membrane integrity and stimulate lipoxygenase activities, thereby catalyzing peroxidation of unsaturated fatty acids in the membranes (16, 58). Linoleic and linolenic acids are the most abundant unsaturated fatty acids in plants. Similar to BULK and ION treatments, CdS-QDs exposure downregulated a few proteins involved in linoleic acid metabolism in the roots. However, α-linolenic acid metabolism was upregulated by CdS-QDs and BULK exposures. Interestingly, the upregulation of fatty acid β-oxidation was unique to the CdS-QDs exposure.

CdS-QD activate stress response in soybean plants

Plant hormones, jasmonic acid and salicyclic acid, are important signaling molecules that respond to heavy metal induced oxidative stress (48). In this study, jasmonic acid signaling cascade was upregulated in the soybean roots exposed to CdS-QDs and BULK treatments. In addition, Cd exposures also enhanced the expression of a pathogenicity-related gene (PR1), which induces systemic acquired resistance by activating the salicylic acid signaling pathway (59). This is in agreement with the findings by Marmiroli et al. in *A. thaliana*, where PR1 was upregulated in response to 80 μg/ml CdS-QDs exposure (18). Enhanced expression of genes regulating salicylic acid signaling pathways, including PR1, in response to $CdCl_2$ at 10 and 100 μM was also reported in the leaves and roots of *A. thaliana* and *Triticum aestivum,* respectively (59, 60).

The CdS-QDs and BULK exposures also upregulated the phenylpropanoid pathway in soybeans. Phenylalanine (*Phe*), *Trp*, and *Tyr* are initiated from metabolites of glycolysis and pentose phosphate pathway via the shikimate pathway and are involved in the biosynthesis of

various metabolites including phenylpropanoids including lignin and flavonoids. CdS-QD exposure has been reported to induce lignification, as a final product of the phenylpropanoid pathway in soybeans (12) and *A. thaliana* (61). The plants exposed to ION treatments utilized peroxidases to cope with the oxidative stress; however, when exposed to CdS-QDs and BULK, the cells were rescued via GSH metabolism. Both CdS-QD and BULK exposures resulted in upregulation of GSH metabolism in the roots, and GGCT2;1 gene that recycles *Glu* for GSH biosynthesis, were downregulated. This was further confirmed by over-accumulation of *Glu* in the CdS-QD-treated roots suggesting poor utilization of the *Glu*. QD-PVP exposure resulted in maximum downregulation of GGCT2;1 and upregulation of PR1 and SULTR4;2 among all the treatments, in addition to a significant increase in MT2 expression. The downregulation of GGCT2;1 in QD-PVP plants hinders the recycling of *Glu* and turnover of GSH after detoxification processes in response to a high concentration of Cd in the shoots, ultimately leading to decreased shoot biomass. The downregulation of GGCT2;1 may impair the GSH homeostasis leading to enhanced transcription of SULTR4;2 to regulate sulfate assimilation for production of S-containing secondary metabolites like glucosinolates, responsible for defense mechanisms in soybean plants (62, 63).

CONCLUSION

This study for the first time revealed the role of unique transmembrane transporters in soybean plants in the uptake of differentially coated CdS-QDs and modulate nutrient acquisition by utilizing omic approaches. Integration of discovery proteomics with targeted analysis of metabolites and gene expression in soybean roots identified glycolysis, TCA cycle and fatty acid oxidation as the major metabolic pathways that were affected by CdS-QD exposure. The stress response in the CdS-QD exposed plants were similar to bulk-sized CdS exposures. The omic

platforms provided supporting evidences on the impact on jasmonic acid/salicylic acid signaling pathway, GSH metabolism, and phenylpropanoid pathway in the soybean plants exposed to CdS-QDs and bulk-CdS exposures. This study provides strong evidence that the response of CdS-QDs exposure is not entirely due to leaching of ions, and it is heavily influenced by the surface coating on the nanoparticles. A holistic understanding of the underlying molecular mechanisms and the factors influencing the uptake and biological response would thus allow safer production and application of quantum dots in the future.

ACKNOWLEDGEMENT

This work was supported by the National Science Foundation and the U.S. Environmental Protection Agency under NSF-EF0830117 and NSF 1901515. Any opinions, findings, conclusions, or recommendations expressed in this material are those of the authors and do not necessarily reflect the views of the funding agencies. AAK appreciates Agilent Technologies for their Agilent Thought Leader Award. LP acknowledges the support of the project INTENSE, grant no. 652515. JCW acknowledges USDA NIFA Hatch CONH00147. We also acknowledge Prof. Nelson Marmiroli, Shima Rayatpisheh and Yasaman Jami-Alahmadi for their assistance.

REFERENCES

1. Giese B, Klaessig F, Park B, Kaegi R, Steinfeldt M, Wigger H, et al. Risks, Release and Concentrations of Engineered Nanomaterial in the Environment. Scientific Reports. 2018;8(1):1565.
2. Nel AE, Mädler L, Velegol D, Xia T, Hoek EMV, Somasundaran P, et al. Understanding biophysicochemical interactions at the nano–bio interface. Nature Materials. 2009;8:543.
3. Fadeel B, Farcal L, Hardy B, Vázquez-Campos S, Hristozov D, Marcomini A, et al. Advanced tools for the safety assessment of nanomaterials. Nature Nanotechnology. 2018;13(7):537-43.

4. Hossain Z, Mustafa G, Komatsu S. Plant Responses to Nanoparticle Stress. International journal of molecular sciences. 2015;16(11):26644-53.
5. Gioria S, Lobo Vicente J, Barboro P, La Spina R, Tomasi G, Urbán P, et al. A combined proteomics and metabolomics approach to assess the effects of gold nanoparticles in vitro. Nanotoxicology. 2016;10(6):736-48.
6. Shin TH, Lee DY, Lee H-S, Park HJ, Jin MS, Paik M-J, et al. Integration of metabolomics and transcriptomics in nanotoxicity studies. BMB reports. 2018;51(1):14-20.
7. Mo D, Hu L, Zeng G, Chen G, Wan J, Yu Z, et al. Cadmium-containing quantum dots: properties, applications, and toxicity. Applied Microbiology and Biotechnology. 2017;101(7):2713-33.
8. Jin S, Hu Y, Gu Z, Liu L, Wu H-C. Application of Quantum Dots in Biological Imaging. Journal of Nanomaterials. 2011;2011:13.
9. Wang Y, Nowack B. Dynamic probabilistic material flow analysis of nano-SiO2, nano iron oxides, nano-CeO2, nano-Al2O3, and quantum dots in seven European regions. Environmental Pollution. 2018;235:589-601.
10. Contreras EQ, Cho M, Zhu H, Puppala HL, Escalera G, Zhong W, et al. Toxicity of quantum dots and cadmium salt to Caenorhabditis elegans after multigenerational exposure. Environmental science & technology. 2013;47(2):1148-54.
11. Modlitbová P, Novotný K, Pořízka P, Klus J, Lubal P, Zlámalová-Gargošová H, et al. Comparative investigation of toxicity and bioaccumulation of Cd-based quantum dots and Cd salt in freshwater plant Lemna minor L. Ecotoxicology and Environmental Safety. 2018;147:334-41.
12. Majumdar S, Ma C, Villani M, Zuverza-Mena N, Pagano L, Huang Y, et al. Surface coating determines the response of soybean plants to cadmium sulfide quantum dots. NanoImpact. 2019:100151.
13. Priester JH, Stoimenov PK, Mielke RE, Webb SM, Ehrhardt C, Zhang JP, et al. Effects of Soluble Cadmium Salts Versus CdSe Quantum Dots on the Growth of Planktonic Pseudomonas aeruginosa. Environmental Science & Technology. 2009;43(7):2589-94.
14. Jin L, Wang X. Cadmium absorption and transportation pathways in plants AU - Song, Yu. International Journal of Phytoremediation. 2017;19(2):133-41.
15. Wang Y, Xu L, Shen H, Wang J, Liu W, Zhu X, et al. Metabolomic analysis with GC-MS to reveal potential metabolites and biological pathways involved in Pb &Cd stress response of radish roots. Scientific reports. 2015;5:18296-.
16. Chen Z, Zhu D, Wu J, Cheng Z, Yan X, Deng X, et al. Identification of differentially accumulated proteins involved in regulating independent and combined osmosis and cadmium stress response in Brachypodium seedling roots. Scientific Reports. 2018;8(1):7790.
17. Zhu G, Xiao H, Guo Q, Zhang Z, Zhao J, Yang D. Effects of cadmium stress on growth and amino acid metabolism in two Compositae plants. Ecotoxicology and Environmental Safety. 2018;158:300-8.
18. Marmiroli M, Pagano L, Savo Sardaro ML, Villani M, Marmiroli N. Genome-Wide Approach in Arabidopsis thaliana to Assess the Toxicity of Cadmium Sulfide Quantum Dots. Environmental Science & Technology. 2014;48(10):5902-9.
19. Al-Salim N, Barraclough E, Burgess E, Clothier B, Deurer M, Green S, et al. Quantum dot transport in soil, plants, and insects. Science of The Total Environment. 2011;409(17):3237-48.

20. Liu J, Katahara J, Li G, Coe-Sullivan S, Hurt RH. Degradation products from consumer nanocomposites: a case study on quantum dot lighting. Environmental science & technology. 2012;46(6):3220-7.
21. Lee W-M, An Y-J. Evidence of three-level trophic transfer of quantum dots in an aquatic food chain by using bioimaging. Nanotoxicology. 2015;9(4):407-12.
22. Koo Y, Wang J, Zhang Q, Zhu H, Chehab EW, Colvin VL, et al. Fluorescence Reports Intact Quantum Dot Uptake into Roots and Translocation to Leaves of Arabidopsis thaliana and Subsequent Ingestion by Insect Herbivores. Environmental Science & Technology. 2015;49(1):626-32.
23. Lee B-T, Kim H-A, Williamson JL, Ranville JF. Bioaccumulation and in-vivo dissolution of CdSe/ZnS with three different surface coatings by Daphnia magna. Chemosphere. 2016;143:115-22.
24. Kim E, Hwang S, Lee I. SoyNet: a database of co-functional networks for soybean Glycine max. Nucleic acids research. 2017;45(D1):D1082-D9.
25. Villani M, Calestani D, Lazzarini L, Zanotti L, Mosca R, Zappettini A. Extended functionality of ZnO nanotetrapods by solution-based coupling with CdS nanoparticles. Journal of Materials Chemistry. 2012;22(12):5694-9.
26. Majumdar S, Almeida IC, Arigi EA, Choi H, VerBerkmoes NC, Trujillo-Reyes J, et al. Environmental Effects of Nanoceria on Seed Production of Common Bean (Phaseolus vulgaris): A Proteomic Analysis. Environmental Science & Technology. 2015;49(22):13283-93.
27. Kaiser P, Wohlschlegel J. Identification of Ubiquitination Sites and Determination of Ubiquitin-Chain Architectures by Mass Spectrometry. Methods in Enzymology. 399: Academic Press; 2005. p. 266-77.
28. Perez-Riverol Y, Csordas A, Bai J, Bernal-Llinares M, Hewapathirana S, Kundu DJ, et al. The PRIDE database and related tools and resources in 2019: improving support for quantification data. Nucleic acids research. 2019;47(D1):D442-D50.
29. Cox J, Mann M. MaxQuant enables high peptide identification rates, individualized p.p.b.-range mass accuracies and proteome-wide protein quantification. Nature Biotechnology. 2008;26:1367.
30. Tyanova S, Temu T, Sinitcyn P, Carlson A, Hein MY, Geiger T, et al. The Perseus computational platform for comprehensive analysis of (prote)omics data. Nature Methods. 2016;13:731.
31. The UniProt C. UniProt: a worldwide hub of protein knowledge. Nucleic Acids Research. 2018;47(D1):D506-D15.
32. Morishima K, Tanabe M, Furumichi M, Kanehisa M, Sato Y. New approach for understanding genome variations in KEGG. Nucleic Acids Research. 2018;47(D1):D590-D5.
33. Chong J, Soufan O, Li C, Caraus I, Li S, Bourque G, et al. MetaboAnalyst 4.0: towards more transparent and integrative metabolomics analysis. Nucleic Acids Research. 2018;46(W1):W486-W94.
34. Szklarczyk D, Morris JH, Cook H, Kuhn M, Wyder S, Simonovic M, et al. The STRING database in 2017: quality-controlled protein-protein association networks, made broadly accessible. Nucleic acids research. 2017;45(D1):D362-D8.
35. Shannon P, Markiel A, Ozier O, Baliga NS, Wang JT, Ramage D, et al. Cytoscape: a software environment for integrated models of biomolecular interaction networks. Genome research. 2003;13(11):2498-504.

36. Radic S, Geitner NK, Podila R, Käkinen A, Chen P, Ke PC, et al. Competitive Binding of Natural Amphiphiles with Graphene Derivatives. Scientific Reports. 2013;3:2273.
37. Hauck OK, Scharnberg J, Escobar NM, Wanner G, Giavalisco P, Witte C-P. Uric Acid Accumulation in an Arabidopsis Urate Oxidase Mutant Impairs Seedling Establishment by Blocking Peroxisome Maintenance. The Plant Cell. 2014;26(7):3090.
38. Sharma A, Shahzad B, Rehman A, Bhardwaj R, Landi M, Zheng B. Response of Phenylpropanoid Pathway and the Role of Polyphenols in Plants under Abiotic Stress. Molecules. 2019;24(13):2452.
39. Piślewska M, Bednarek P, Stobiecki M, Zielińska M, Wojtaszek P. Cell wall-associated isoflavonoids and β-glucosidase activity in Lupinus albus plants responding to environmental stimuli. Plant, Cell & Environment. 2002;25(1):20-40.
40. Hussain RMF, Sheikh AH, Haider I, Quareshy M, Linthorst HJM. Arabidopsis WRKY50 and TGA Transcription Factors Synergistically Activate Expression of PR1. Frontiers in plant science. 2018;9:930-.
41. Jozefczak M, Remans T, Vangronsveld J, Cuypers A. Glutathione is a key player in metal-induced oxidative stress defenses. International journal of molecular sciences. 2012;13(3):3145-75.
42. Paulose B, Chhikara S, Coomey J, Jung H-I, Vatamaniuk O, Dhankher OP. A γ-glutamyl cyclotransferase protects Arabidopsis plants from heavy metal toxicity by recycling glutamate to maintain glutathione homeostasis. The Plant cell. 2013;25(11):4580-95.
43. Tehseen M, Cairns N, Sherson S, Cobbett CS. Metallochaperone-like genes in Arabidopsis thaliana. Metallomics. 2010;2(8):556-64.
44. Tzin V, Galili G. The Biosynthetic Pathways for Shikimate and Aromatic Amino Acids in Arabidopsis thaliana. The arabidopsis book. 2010;8:e0132-e.
45. Leszczyszyn OI, Imam HT, Blindauer CA. Diversity and distribution of plant metallothioneins: a review of structure, properties and functions. Metallomics. 2013;5(9):1146-69.
46. Villiers F, Ducruix C, Hugouvieux V, Jarno N, Ezan E, Garin J, et al. Investigating the plant response to cadmium exposure by proteomic and metabolomic approaches. PROTEOMICS. 2011;11(9):1650-63.
47. Song Y, Jin L, Wang X. Cadmium absorption and transportation pathways in plants. International Journal of Phytoremediation. 2017;19(2):133-41.
48. Zhou M, Zheng S, Liu R, Lu J, Lu L, Zhang C, et al. Comparative analysis of root transcriptome profiles between low- and high-cadmium-accumulating genotypes of wheat in response to cadmium stress. Funct Integr Genomics. 2019;19(2):281-94.
49. Zhao J, Zhou H, Li X. UBIQUITIN-SPECIFIC PROTEASE16 interacts with a HEAVY METAL ASSOCIATED ISOPRENYLATED PLANT PROTEIN27 and modulates cadmium tolerance. Plant Signaling & Behavior. 2013;8(10):e25680.
50. Fang X, Wang L, Deng X, Wang P, Ma Q, Nian H, et al. Genome-wide characterization of soybean P 1B -ATPases gene family provides functional implications in cadmium responses. BMC Genomics. 2016;17(1):1-15.
51. Bernal M, Testillano P, Alfonso M, Risueno M-C, Picorel R, Yruela I. Identification and subcellular localization of the soybean copper P1B-ATPase GmHMA8 transporter2007. 46-58 p.
52. Qiu R, Tang Y-T, Zeng X-W, Thangavel P, Tang L, Gan Y-Y, et al. Progress in Botany. 2012. p. 127-59.

53. Cailliatte R, Lapeyre B, Briat J-F, Mari S, Curie C. The NRAMP6 metal transporter contributes to cadmium toxicity. Biochemical Journal. 2009;422(2):217.
54. Srivastava AK, Penna S, Nguyen DV, Tran L-SP. Multifaceted roles of aquaporins as molecular conduits in plant responses to abiotic stresses. Critical Reviews in Biotechnology. 2016;36(3):389-98.
55. Yue L, Ma C, Zhan X, White JC, Xing B. Molecular mechanisms of maize seedling response to La2O3 NP exposure: water uptake, aquaporin gene expression and signal transduction. Environmental Science: Nano. 2017;4(4):843-55.
56. Taiz L, Zeiger E. Plant Physiology. Fifth ed: Sinauer Associates, Inc; 2010.
57. Xie Y, Hu L, Du Z, Sun X, Amombo E, Fan J, et al. Effects of cadmium exposure on growth and metabolic profile of bermudagrass [Cynodon dactylon (L.) Pers]. PloS one. 2014;9(12):e115279-e.
58. Ben Ammar W, Nouairi I, Zarrouk M, Jemal F. The effect of cadmium on lipid and fatty acid biosynthesis in tomato leaves. Biologia. 2008;63(1):86-93.
59. Zhou M, Zheng S, Liu R, Lu J, Lu L, Zhang C, et al. Comparative analysis of root transcriptome profiles between low- and high-cadmium-accumulating genotypes of wheat in response to cadmium stress. Functional & Integrative Genomics. 2018.
60. Cabot C, Gallego B, Martos S, Barceló J, Poschenrieder C. Signal cross talk in Arabidopsis exposed to cadmium, silicon, and Botrytis cinerea. Planta. 2013;237(1):337-49.
61. Marmiroli M, Imperiale D, Pagano L, Villani M, Zappettini A, Marmiroli N. The Proteomic Response of Arabidopsis thaliana to Cadmium Sulfide Quantum Dots, and Its Correlation with the Transcriptomic Response. 2015;6(1104).
62. Maruyama-Nakashita A, Nakamura Y, Tohge T, Saito K, Takahashi H. Arabidopsis SLIM1 is a central transcriptional regulator of plant sulfur response and metabolism. The Plant cell. 2006;18(11):3235-51.
63. Kumar S, Kaur A, Chattopadhyay B, Bachhawat Anand K. Defining the cytosolic pathway of glutathione degradation in Arabidopsis thaliana: role of the ChaC/GCG family of γ-glutamyl cyclotransferases as glutathione-degrading enzymes and AtLAP1 as the Cys-Gly peptidase. Biochemical Journal. 2015;468(1):73.

Table 1. Biological pathways enriched in soybean roots exposed to 200 µg/ml CdS-QD treatments, derived from shotgun proteomics analysis (False discover rate, FDR ≤ 0.01)

ENRICHED KEGG Pathway	FDR	Number of enriched genes
UPREGULATED		
Biosynthesis of secondary metabolites	2.26E-44	64
Carbon metabolism	4.51E-27	29
Biosynthesis of amino acids	1.50E-20	23
Glycolysis / Gluconeogenesis	3.24E-15	16
Fatty acid degradation	1.07E-11	10
Citrate cycle (TCA cycle)	2.03E-11	10
Peroxisome	2.20E-11	11
Pyruvate metabolism	2.22E-09	10
Glyoxylate and dicarboxylate metabolism	2.49E-09	9
2-Oxocarboxylic acid metabolism	5.60E-09	8
α -Linolenic acid metabolism	7.76E-09	8
Glutathione metabolism	1.57E-08	9
Isoflavonoid biosynthesis	3.15E-08	6
Biosynthesis of unsaturated fatty acids	1.55E-06	5
Valine, leucine and isoleucine degradation	2.97E-06	6
Pentose phosphate pathway	6.26E-06	6
Tryptophan metabolism	2.81E-05	5
Phenylpropanoid biosynthesis	3.71E-05	8
Propanoate metabolism	1.30E-04	4
Carbon fixation in photosynthetic organisms	1.30E-04	5
Phenylalanine metabolism	3.80E-04	4
Tyrosine metabolism	4.80E-04	4
Purine metabolism	7.30E-04	6
Tropane, piperidine and pyridine alkaloid biosynthesis	0.001	3
Glycine, serine and threonine metabolism	0.0013	4
Fructose and mannose metabolism	0.0018	4
Arginine biosynthesis	0.002	3
C5-Branched dibasic acid metabolism	0.002	2
Protein processing in endoplasmic reticulum	0.002	6
Fatty acid biosynthesis	0.0036	3
Ascorbate and aldarate metabolism	0.004	3
DOWNREGULATED		
Ribosome	1.68E-08	12
Metabolic pathways	1.12E-05	23
Aminoacyl-tRNA biosynthesis	3.80E-04	4
Endocytosis	5.60E-04	6
Galactose metabolism	6.80E-04	4
Linoleic acid metabolism	0.0011	3
Starch and sucrose metabolism	0.0013	5
Ribosome biogenesis in eukaryotes	0.0013	4
Tyrosine metabolism	0.0038	3
Fatty acid degradation	0.0044	3

Figure legends (The figures uploaded in separate files)

Figure 1. Venn diagram of proteins identified in soybean roots (a) exposed to CdS-QDs (QD-BARE, QD-TOPO, QD-PVP, QD-MAA, and QD-GLY) treatments; and (b) exposed to CTRL, ION, BULK and proteins found common between all CdS-QD treatments.

Figure 2. Differentially accumulated proteins (DAPs) in the roots exposed to CTRL, ION, BULK and CdS-QDs (a) Principal component analysis of DAPs identified by one-way ANOVA with Benjamini Hochberg FDR ≤ 0.05, (b) Number of DAPs in ION, BULK and CdS-QDs compared to CTRL, (c) Venn diagram of DAPs in ION, BULK and CdS-QD-treated roots, (d) Venn diagram of the DAPs with increased and decreased abundances in the roots exposed to CdS-QDs with respect to CTRL.

Figure 3. Hierarchical clustering analysis of the ANOVA significant proteins in the soybean roots exposed to CTRL, ION, BULK and CdS-QDs (a) Heat map demonstrating the clusters with the abundance scale shown in the legend; (b) Abundance pattern of the differentially accumulated proteins in three clusters.

Figure 4. Bar plot illustrating log-normalized relative fold change in gene expression in (a) Roots, and (b) Shoots of soybean plants exposed to ION, BULK, and CdS-QD treatments with respect to CTRL plants.

Figure 5. Impact on metabolites in the roots from soybean plants exposed to CTRL, ION, BULK, and CdS-QDs. (a) PCA score plot, and (b) PLS-DA score plot of metabolites identified in the leaves, (c) Fold change of the metabolites that were affected by all CdS-QD exposures with respect to CTRL.

Figure 6. Impact on metabolites in the leaves from soybean plants exposed to CTRL, ION, BULK, and CdS-QDs. (a) PCA score plot, and (b) three-dimensional PLS-DA score plot of metabolites identified in the leaves, (c) Important features identified among the 26 leaf metabolites identified by PLS-DA, the colored boxes indicate the relative concentrations of the corresponding metabolite in each group, (d) Heat map showing hierarchical clustering of the 18 differentially accumulated metabolites at FDR ≤ 0.05. The color bar shows the increase (red) and decrease (green) in the abundance of the metabolites.

Figure 7. Protein-protein interaction and network analysis of the differentially regulated proteins, metabolites and genes in the soybean roots exposed to CdS-QDs compared to CTRL. The nodes represent the biological entities and the arrowed edges represent the interactions between them with a confidence score of ≥ 0.7.

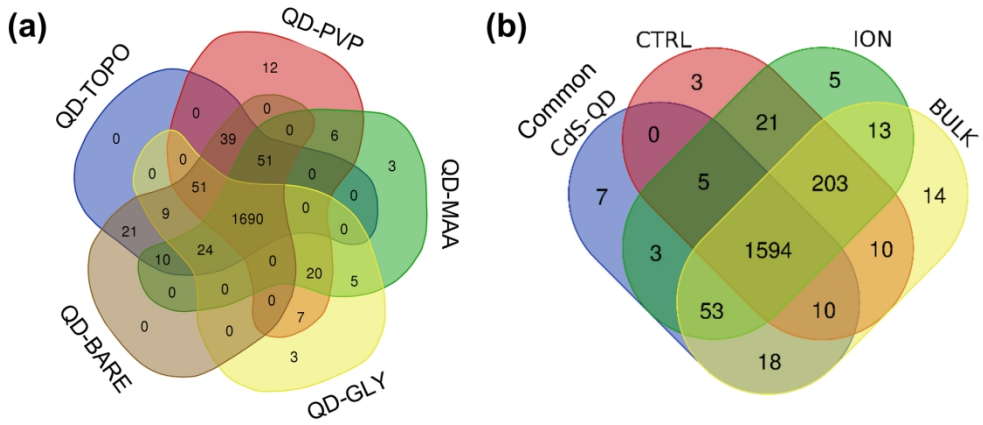

Venn diagram of proteins identified in soybean roots (a) exposed to CdS-QDs (QD-BARE, QD-TOPO, QD-PVP, QD-MAA, and QD-GLY) treatments; and (b) exposed to CTRL, ION, BULK and proteins found common between all CdS-QD treatments.

170x78mm (300 x 300 DPI)

(a)

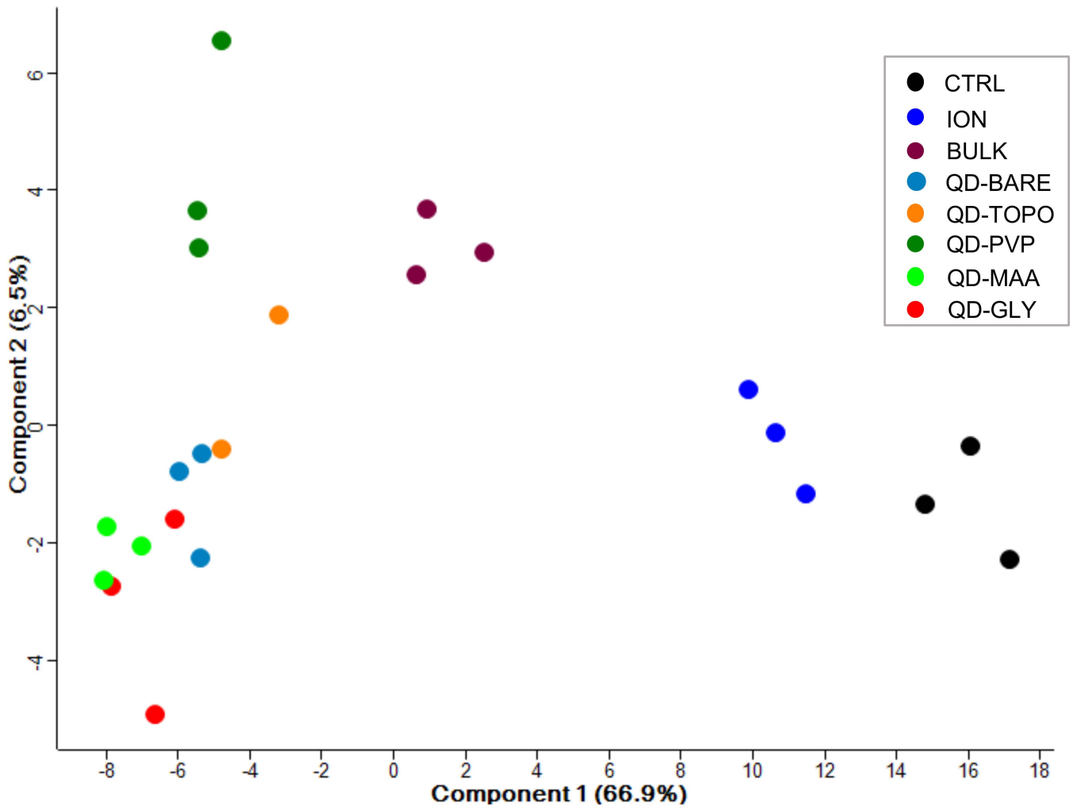
CTRL
ION
BULK
QD-BARE
QD-TOPO
QD-PVP
QD-MAA
QD-GLY
Component 2 (6.5%)
Component 1 (66.9%)

(b)

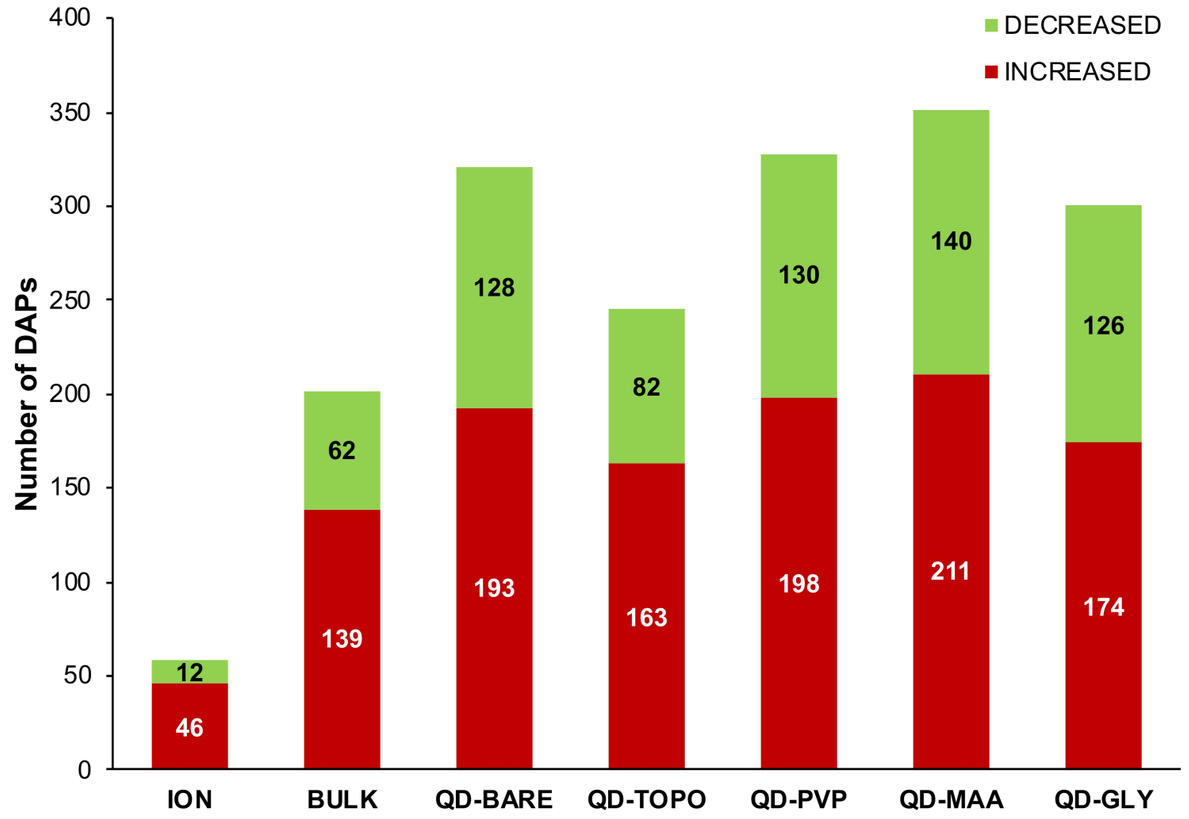
DECREASED
INCREASED
Number of DAPs
ION
BULK
QD-BARE
QD-TOPO
QD-PVP
QD-MAA
QD-GLY
12
46
62
139
128
193
82
163
130
198
140
211
126
174

(c)

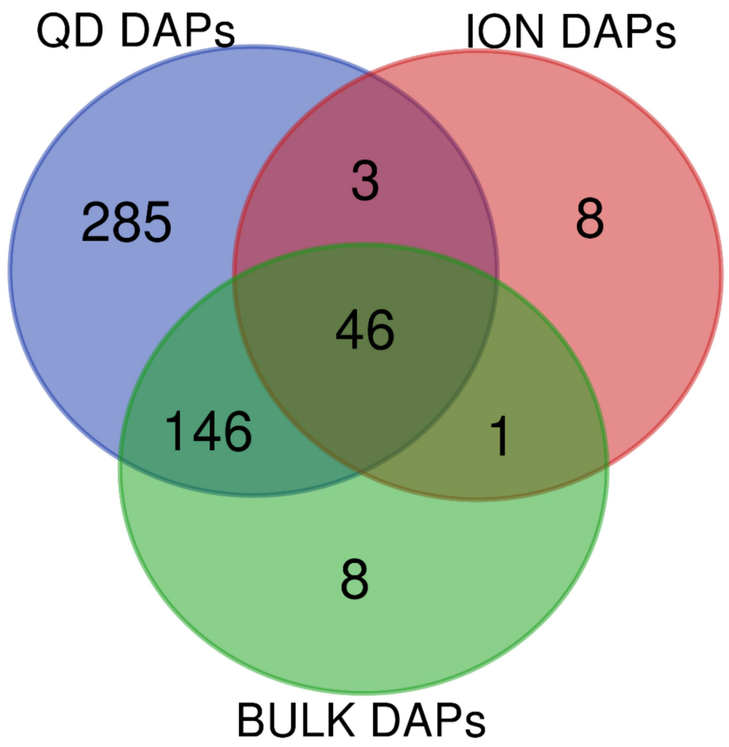
QD DAPs
ION DAPs
BULK DAPs
285
3
8
46
146
1
8

(d)

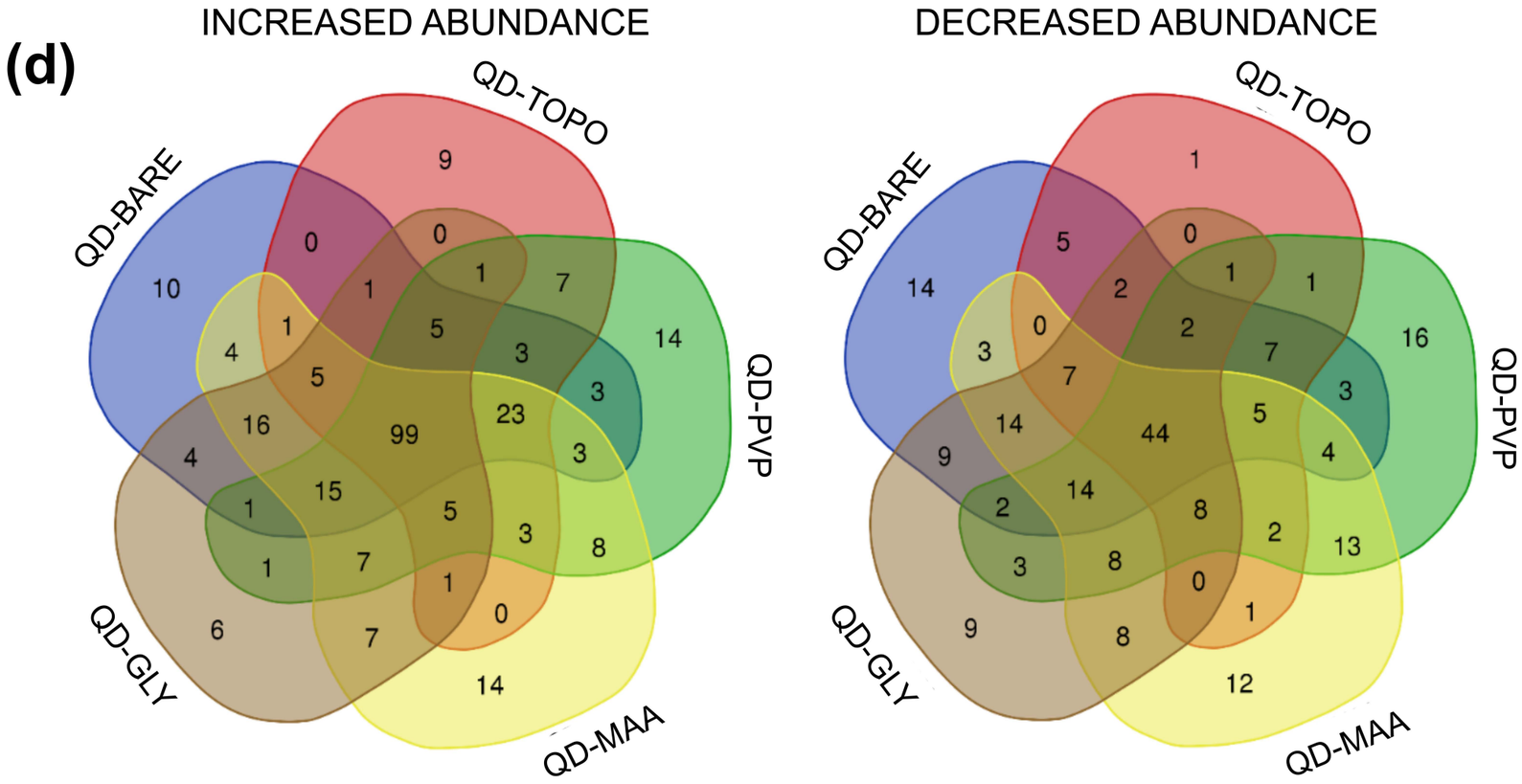
INCREASED ABUNDANCE
DECREASED ABUNDANCE
QD-BARE
QD-TOPO
QD-PVP
QD-GLY
QD-MAA

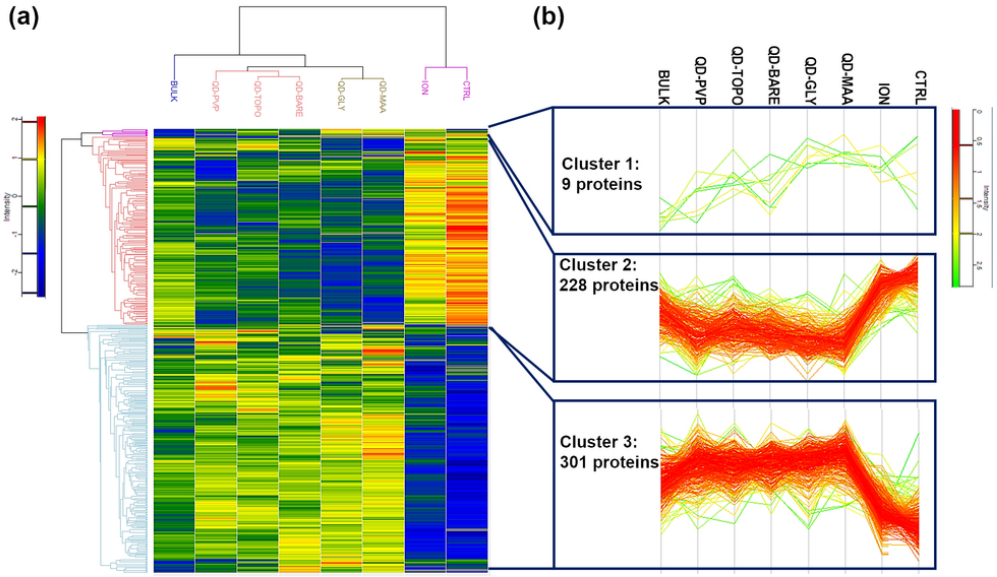

Hierarchical clustering analysis of the ANOVA significant proteins in the soybean roots exposed to CTRL, ION, BULK and CdS-QDs (a) Heat map demonstrating the clusters with the abundance scale shown in the legend; (b) Abundance pattern of the differentially accumulated proteins in three clusters.

83x48mm (300 x 300 DPI)

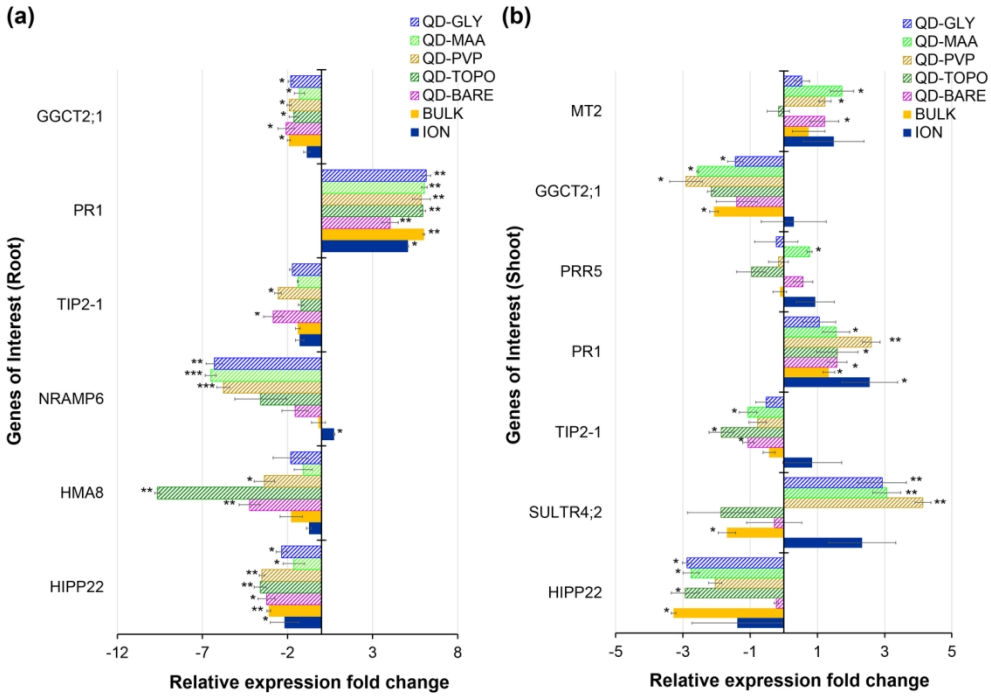

Bar plot illustrating log-normalized relative fold change in gene expression in (a) Roots, and (b) Shoots of soybean plants exposed to ION, BULK, and CdS-QD treatments with respect to CTRL plants.

134x96mm (300 x 300 DPI)

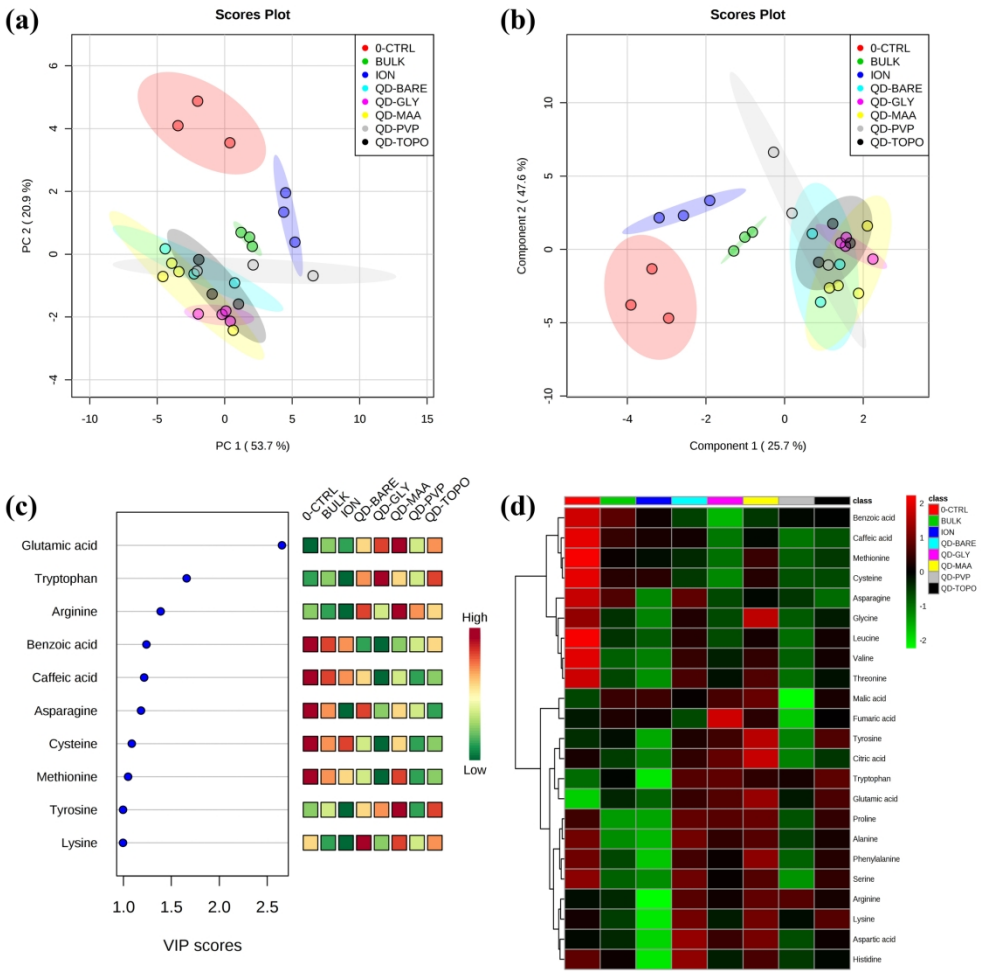

Impact on metabolites in the roots from soybean plants exposed to CTRL, ION, BULK, and CdS-QDs. (a) PCA score plot, and (b) PLS-DA score plot of metabolites identified in the leaves, (c) Fold change of the metabolites that were affected by all CdS-QD exposures with respect to CTRL.

216x212mm (300 x 300 DPI)

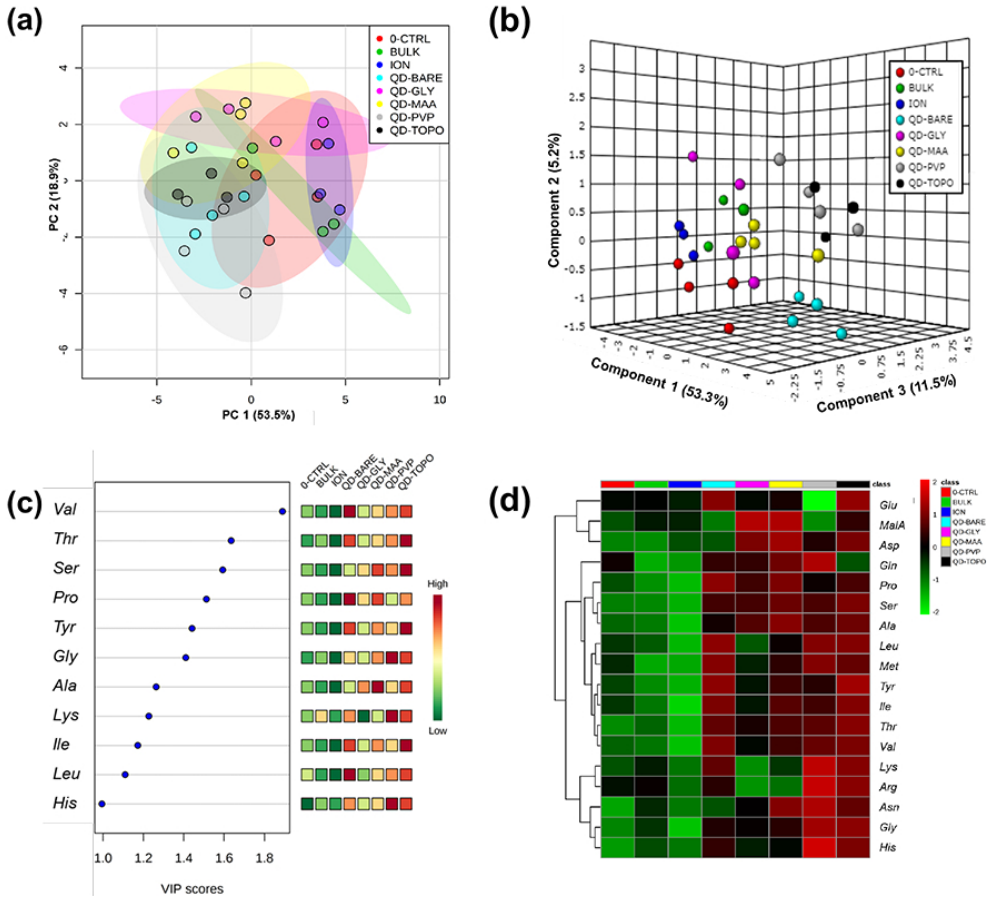

Impact on metabolites in the leaves from soybean plants exposed to CTRL, ION, BULK, and CdS-QDs. (a) PCA score plot, and (b) three-dimensional PLS-DA score plot of metabolites identified in the leaves, (c) Important features identified among the 26 leaf metabolites identified by PLS-DA, the colored boxes indicate the relative concentrations of the corresponding metabolite in each group, (d) Heat map showing hierarchical clustering of the 18 differentially accumulated metabolites at FDR ≤ 0.05. The color bar shows the increase (red) and decrease (green) in the abundance of the metabolites.

76x69mm (300 x 300 DPI)

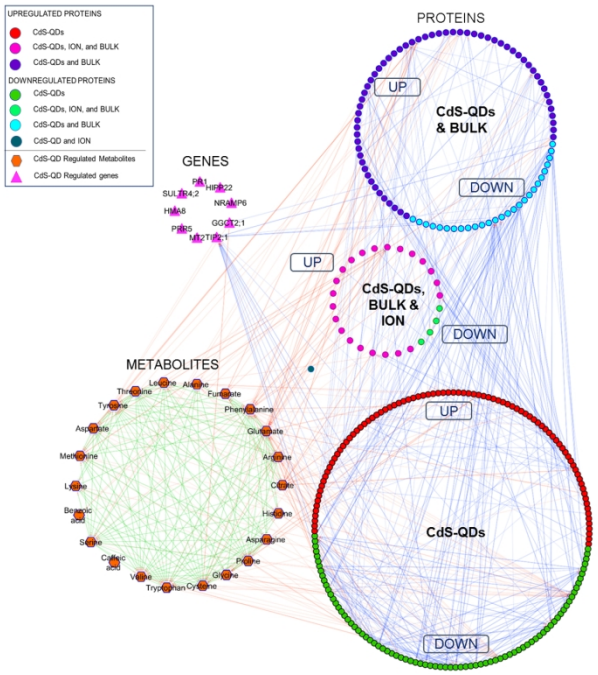

Modulated Pathways	False discovery rate	Number of enriched genes
Metabolic pathways	1.04E-44	101
Carbon metabolism	1.30E-23	32
Biosynthesis of amino acids	2.73E-16	24
Glycolysis / Gluconeogenesis	6.17E-15	19
Fatty acid degradation	2.07E-13	13
Peroxisome	6.19E-10	12
Pyruvate metabolism	3.23E-09	12
Citrate cycle (TCA cycle)	3.75E-09	10
alpha-Linolenic acid metabolism	4.34E-08	9
Glutathione metabolism	1.91E-07	10
Glyoxylate and dicarboxylate metabolism	2.51E-07	9
2-Oxocarboxylic acid metabolism	3.54E-07	8
Isoflavonoid biosynthesis	8.76E-07	6
Phenylpropanoid biosynthesis	1.59E-06	12
Tyrosine metabolism	3.00E-06	7
Valine, leucine and isoleucine degradation	5.50E-06	7
Pentose phosphate pathway	1.29E-05	7
Biosynthesis of unsaturated fatty acids	2.14E-05	5
Phenylalanine metabolism	2.32E-05	6
Tryptophan metabolism	2.63E-05	6
Ribosome	4.02E-05	12
beta-Alanine metabolism	5.57E-05	6
Glycine, serine and threonine metabolism	1.40E-04	6
Carbon fixation in photosynthetic organisms	1.40E-04	6
Ascorbate and aldarate metabolism	2.40E-04	5
Amino sugar and nucleotide sugar metabolism	2.40E-04	8
Protein processing in endoplasmic reticulum	3.90E-04	9
Galactose metabolism	8.10E-04	5
Propanoate metabolism	8.10E-04	4
Endocytosis	8.90E-04	8
Fatty acid biosynthesis	0.002	4
Purine metabolism	0.002	7
Aminoacyl-tRNA biosynthesis	0.0026	4
Linoleic acid metabolism	0.0053	3
C5-Branched dibasic acid metabolism	0.0059	2
Arginine biosynthesis	0.0087	3
Fructose and mannose metabolism	0.0107	4
Phenylalanine, tyrosine and tryptophan biosynthesis	0.0132	3
Glycosphingolipid biosynthesis - globo and isoglobo series	0.0132	2
Ribosome biogenesis in eukaryotes	0.0141	4
Ubiquinone and other terpenoid-quinone biosynthesis	0.0209	3
Starch and sucrose metabolism	0.0229	5
Other glycan degradation	0.0242	2
Pentose and glucuronate interconversions	0.0301	4
Ether lipid metabolism	0.0446	2

Protein-protein interaction and network analysis of the differentially regulated proteins, metabolites and genes in the soybean roots exposed to CdS-QDs compared to CTRL. The nodes represent the biological entities and the arrowed edges represent the interactions between them with a confidence score of ☐ 0.7.